Characterization and Autotuning of Magnetic Resonance based Through-the-body Communications

Hirsa Kia[a], Krishna Kant[b,1]

[a]*Department of Computer & Information Sciences, Temple University, Philadelphia, PA 19122, USA*
[b]*Department of Computer & Information Sciences, Temple University, Philadelphia, PA 19122, USA*

Abstract

In this paper we explore the Magnetic Resonance Coupling (MRC) based communication for small intrabody network of nodes designed to manage chronic illnesses. We demonstrate that MRC is well-suited for such networks and shows much lower attenuation than in the air, and can reach distances of up to a meter with only 20 db loss. Although inbody experiments are not possible, we provide ample evidence that the results obtained from onbody experiments provide a good approximation to the propagation characteristics. In particular, we compare measurement results against detailed intra-body propagation results and find an excellent match. We also show that the best propagation characteristic occur in the 25-30 MHz frequency range. Based on a set of real on-body measurements, we devise an attenuation model that allows for multiple receivers, and show that the model can generally predict the results within about 1 db. We also show that the propagation characteristics are affected by the physiological characteristics of the body, and thus could drift over both short term (e.g., normal fluctuations) and long term (e.g., effect of aging or diseases). We present an autotuning mechanism have the MRC links operating optimally in spite of such fluctuations.

Keywords: Magnetic Resonance Coupling, Ultrasonic Coupling, Intra-body network, Sim4Life, Path-loss, Q-factor tuning

1. Introduction

There is an increasing array of human assistive technologies that generally require sensing some vital parameters and accordingly applying or simply recommending some corrective action. The signal may not necessarily be captured in the same place where the action occurs, thereby requiring a small wireless network that can collect all signals efficiently without interference, fuse them together, and decide upon the appropriate action. Such networks are crucial for managing chronic conditions and may include some sensors attached to the skin while others are implanted.

Thus, through-the-body wireless communications (TBWC) become essential to operate these networks. Furthermore, since long-lasting batteries are usually too big for implants, a wireless power transfer (WPT) to the nodes is also required. For the most part, the WPT and communications face similar issues and have resulted in a significant amount of research in Human Body Communications (HBC) technologies.

The two most promising technologies include Magnetic Resonance Coupling (MRC) and Ultrasonic Coupling (USC). Our experiments in [1, 2] show that among the electromagnetic methods, MRC works much better than others and is very robust against movement, posture, clothing, person to person variations (e.g., build, weight, etc.). We have shown that USC also works quite well [3], but being mechanical in nature, it cannot operate at very high frequencies [4]. It also has difficult acoustic impedance matching issues [5]. Thus, this paper primarily explores MRC.

Both MRC and USC have been explored in the context of both wearables (on-body) and medical uses (on/in-body) both for communication [6, 7] and WPT [8]. For example, Reference [7] considers ear to ear transmission with 2 centimeters air gap on each side, whereas our goal in this study is to consider a truly on-body/in-body with no air-gap as far as possible. The biomedical application of MRC and USC generally consider very short distances (a few mm to few centimeters). Reference [9] explores an USC powered microprobe for electrolyte ablation. Reference [5] develops a USC power receiver for medical devices and discusses MRC power transfer to medical devices. Reference [10] designs a sub-10-pJ/bit 5-Mb/s MRC transceiver.

There are currently very few detailed studies of MRC propagation through the body at frequencies of a few to few tens of MHz range and distances of tens of centimeters. Much of the longer-range characterization models the body either separately for different types of tissues, or by using average dielectric properties, or in the context of very high frequencies. Reference [11], for example, explores both through COMSOL simulation of EM propagation through a homogeneous soft-tissue media and via some experiments on chicken breast. Reference [7] is typical of channel characterization efforts through measurements and simulations. It considers

Email addresses: Hirsa.kia@temple.edu (Hirsa Kia), kkant@temple.edu (Krishna Kant)

propagation over much higher frequency region (50Mhz to 2.4GHz) and uses average dielectric properties of human body, which is not appropriate at lower frequencies.

The novelty of this paper lies in its comprehensive experimental and simulation-based analysis, revealing non-intuitive behaviors within the human body, which have not been thoroughly investigated in previous studies.

The rest of the paper is organized as follows: Section 2 discusses the Magnetic Resonance characteristics and detuning problem. Section 3.1 discusses our detailed experimental and simulation setup, pathloss modeling and tuning control design. The systematic comparison of MRC experiments and simulations on and in the human body, as well as performance of pathloss model and tuning controller, are discussed in section 4. Further discussions are presented in section 5 and the paper is concluded in section 6.

2. Characteristics of MRC Communications

2.1. Magnetic Resonance Coupling (MRC)

MRC involves resonant communication between two coils. Each coil is in series with a capacitor to create a LC tank that has resonance frequency of $f_r = 1/(2\pi\sqrt{LC})$, where L and C are the inductance of coil and the capacitance of the capacitor respectively. For maximum energy transfer efficiency, the transmitter and receiver sides must have matching resonance frequency. Furthermore, to avoid reflections, the two sides also need to have matching impedance (which is purely resistive at resonance frequency).

The TBWC and other applications of MRC, it is assumed that the technology works in the *near-field* regime, often under the name NFMI (near field magnetic induction). In contrast, the traditional RF communications such as BLE are considered as *far field*. The near-field assumption holds when the operating distance d is much smaller than the wavelength λ_r, or more precisely, $d < \lambda_r/2\pi$ [12]. For example, a popular operational frequency for NFMI is 13.56MHz, which is the standard frequency for RFID operation. At this frequency, the near-field limit is 3.5m in the air. In case of far field, the RF power is transferred through Friis equation for propagating EM waves, where electric and magnetic fields are coupled through Faraday's and Ampere's laws in Maxwell's equations. The concept of near-field is really an idealization and characterized by making some assumptions which effectively decouple the magnetic and electric fields. The resonant LC circuits in MRC produce a strong magnetic field and thus a characterization in terms of current flow in the receiver coil due to magnetic induction is an appropriate characterization. Under the near-field assumption, the received power can be easily related with the transmitted power in terms of various parameters [12]. This relationship suggests the following: The induced current increases linearly with the operating frequency and goes down very rapidly with distance h (as h^{-3}). Since the power is proportional to I_r^2, the induced power decays as h^{-6}, which is much faster than the decay for far-field (or RF) case, where the power goes down as h^{-2}. The very rapid decay of the induced power with distance makes the MI technology inherently a small range technology, and this effect is usually more limiting than the near field requirement of $h < \lambda_r/(2\pi)$. The area of transmit and receive coils (proportional to ρ_t^2 and ρ_r^2 respectively) and the number of turns (K_t and K_r) directly influence the mutual inductance and hence the induced current. Increasing the range requires bigger coils and more turns, both of which may be undesirable in applications where small size is required. The frequency and the transmit coil current directly increase the induced current, and hence the overall power consumption (bad) and the range (good).

2.2. MRC Transmission in Other Media

For transmission through materials other than air, it is important to consider their electrical and magnetic properties, which affect the speed of EM propagation ("speed of light"). The latter, denoted by c_r, is given by $c_r = 1/\sqrt{\epsilon \times \mu}$, where ϵ is the electrical permittivity and μ is the magnetic permeability of the media with ϵ_r and μ_r as relative values to the vacuum with permittivity ($\epsilon_0 = 8.85410^{-12}$), and permeability ($\mu_0 = 4\pi \times 10^{-7}$). Since $c_r = \lambda_r \times f$, then a high permittivity or permeability reduces both λ_r and c at a given frequency. For the human body $\mu_r \approx 1$ but ϵ_r varies tremendously from organ to organ [13, 14], with absolute values (including real and imaginary parts) ranging from tens to thousands. The imaginary part results from the conductivity of various organs, which also varies significantly. Furthermore, the permittivity is not constant but goes down with the operating frequency. Table 1 shows a sample of permittivity and conductivity at both 13.56 MHz and 25 MHz and one can see significant variations even within a single organ. Thus the near-field limit inside the body is much smaller than in air. For example, at 13.56MHz, the near field limit for muscle is only about 30 centimeters and at 25 MHz, the limit shrinks to 16.2 centimeters. Thus, the propagation inside the body would operate in the "mid-field" in many practical cases, which yields much more complex and somewhat nonintuitive results that we demonstrate this via measurement and simulation in this paper.

Table 1: Relative Permittivity and Electrical Conductivity of Various Tissues at Different Frequencies[15]

Tissue type	**13.56MHz**		**25MHz**	
	Rel. Permit.	Elec. Cond.	Rel. Permit.	Elec. Cond.
Blood	210.6	1.12	133.1	1.15
Muscle	138.4	0.63	99.3	0.65
Skin (dry)	285.2	0.24	175.7	0.32
Fat (avg.)	25.4	0.06	18.6	0.06

2.3. Detuning Problem in MRC

2.4. Q Factor and Autotuning

MRC works by energy transfer between a transmit and a receive coil separated by the desired communication distance. Each coil has certain inductance L and connected to a capacitor C in series or in parallel, plus a resistor in series to control the current. At any angular frequency $\omega = 2\pi f$, such a circuit has capacitive and inductive reactances, denoted X_C and X_L respectively, given by $X_C = -1/(j\omega)$ and $X_L = j\omega$. Electrical resonance occurs in an AC circuit when the inductive and capacitive reactance are equal, which implies that $\omega_r = \frac{1}{\sqrt{LC}}$. In resonant condition, the impedance of the circuit becomes purely resistive, i.e. $Z = R$.

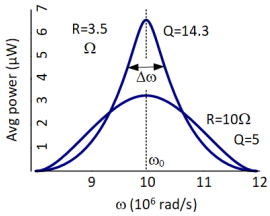

Fig. 1: Resonance Illustration

An important performance indicator of an RLC circuit is the *quality factor* Q, defined as the ratio of the energy stored in the circuit to the energy dissipated by the circuit [16, 17]. It is merely the ratio of reactance and resistance, and is given by $Q = \frac{1}{\omega_r RC}$. The quality factor mainly indicates how efficiently inductors and capacitors in the circuit transfer their energy from the source to the load. The quality factor is also defined as the frequency-to-bandwidth ratio of the resonator, i.e. $Q = \frac{f_r}{\Delta f} = \frac{\omega_r}{\Delta\omega}$ where Δf is the resonance width, i.e. the bandwidth over which the power is greater than half the power at the resonant frequency. $\Delta\omega$ is the corresponding angular half-power bandwidth (See Fig. 1).

The transmit coil can transfer energy to the receive coil because of the mutual inductance between the two coils, denoted M. Thus a time varying voltage V_1 (and corresponding current I_1) in the transmit coil induces a current I_2 in the receiving coil. If the resistor, inductor, and capacitor values of the two coils are (R_1, L_1, C_1) and (R_2, L_2, C_2) respectively, then from Kirchoff's laws, it is easy to conclude that $I_2 = -\frac{j\omega_r M}{R_2} I_1$.

Thus if the transmit data is modulated on the magnetic flux, then the receiver can receive and demodulate the signal. The effectiveness of the mutual coupling is measured by the *coupling coefficient* κ, which can be estimated as

$$\kappa = \frac{M}{\sqrt{L_1 L_2}} \tag{1}$$

If P_1 and P_2 are the transmitted and received power respectively, then the power transfer ratio is given by [17]

$$\frac{P_2}{P_1} = \frac{\omega_r^2 M^2 R_1 R_2}{R_1^2 R_2^2} = \kappa^2 Q_1.Q_2 \tag{2}$$

where Q_1 and Q_2 are the quality factors of the transmit and receive coils respectively. Thus, the power transfer is proportional to the coupling coefficient and the quality factors of the transceiver coils.

It is clear that to maximize energy transfer, both Q_1 and Q_2 should be as high as possible. Unfortunately, a high Q value results in a much sharper peak in the resonance curve as shown in Fig. 1. The key problem with the sharp peak is its stability, since a slight change in the parameters or load variations can change the resonance frequency enough to substantially lower the transfer efficiency. In this paper we devise an autotuning mechanism to ensure that any drift is compensated for and thus the energy transfer stays near its peak.

In general, there could be multiple reasons for drift, some significant, some not. For example, the drift in the capacitance due to aging and temperature variations in the class 1 CoG capacitor used in medical applications is generally quite small or negligible [18]. However, the mounting of the capacitor on the circuit board and the solder can experience changes over time, particularly at higher temperatures [19]. The change could eventually lead to failures; however, our focus here is not failure, but the drift in properties that may occur any time, and certainly much before outright failure.

In addition to the potential drift in the resonance circuit itself, there are other changes whose impact could perturb the resonance significantly. One source of perturbation is the movement of the transmit or receive coil while it is deployed in the patient. Depending on the location, slight movements and orientation changes occur as the body muscles move. These movements would also change the parasitic capacitance contributed by the the body and its contact with the coils. The net effect of these variation is the change in the resonance circuit parameters and thereby a drop in power delivered to the load. Another potential source of perturbation concerns the change in physiological parameter of the person such as blood pressure or heart rate, which we investigate in this paper. While very short-term changes (e.g., 1 minute or less) are not relevant for autotuning, it is desirable to respond to longer term changes either to maintain communication quality (when signal attenuation goes below the nominal value) or to save energy by reducing the transmit energy (when the attenuation is lower than the nominal value).

The problem of "detuning" of resonant circuits due to various impacts has been well recognized and studied in the context of wireless power transfer (WPT). Note that our problem involves integrated WPT and communication which places certain restriction as compared to the pure WPT environment. The main techniques as described below.

The most direct compensation method is to introduce a switchable capacitor/inductor matrix to compensate for the capacitance drift. However, the solutions tend to be rather heavy duty and intended for large power transfer situations. For example, Si et.

al. [20] consider power transfer to pacemaker from outside and describe a way of changing frequency of the operation. It includes both capacitor switching and frequency switching to control power transfer. Lim et al. [21] introduce a self-adaptive capacitor matrix with automated searching for configuration with changing distance between transmit and receive coils.

Another method is to adjust the capacitance via pulse-width modulation (PWM) of the input signal to control how much chance the capacitor gets to charge/discharge in each cycle, which effectively changes its capacitance. Porto et al. [22] do this by using an amplifier, and a double-sided version is discussed in [23]. However, such complexity in unwarranted since voltage controlled capacitors, many built in with push-pull circuit are readily available. Furthermore, PWM can interfere with the communication in the integrated power transfer and communications mechanism that we are interested in. Switching the operating frequency to always correspond to the resonant frequency is a popular method explored in several papers. For example, a self-oscillating switching technique was used in [24]. For our application, frequency switching is undesirable as it is complex and requires the receiver to re-latch to the change frequency to enable proper communication. Another method is to control the phase shift on the receive side by using the semiactive rectifier (SAR) where the trigger modes of the driving signals are altered to achieve matching of the load resistance or reactance. Mai, et al. [25] use both pulse width and the phase shift angle control to provide matching for both the drift and load resistance variations. In our context the rectification will work only for WPT, not communications.

3. Methods

3.1. Experimental and Simulation Setups

3.1.1. Real Measurements

Consistent with our earlier work on the subject, we use flat circular coil that can be placed securely on the skin with an electric gel to make good contact (see Fig. 2). The coils were shielded magnetically on the top so that there is no signal leakage into the air. The transmit and receive coils were identical and placed on different parts of the volunteer's body. We used coils of several different sizes, although most of the results reported here were obtained using a 20 mm diameter case.

The key novelty of the work reported in this paper is the experimental and simulation based study of MRC at different frequencies. A frequency change is nontrivial as it requires a change in inductance and capacitance of the antennas on both transmit and receive sides in a synchronized manner. A simple solution is to use mechanically variable inductors and capacitors (usually changed by turning a screw) and tune them manually. However, we found such variable inductors/capacitors to be rather unstable to the point of being unusable. The voltage controlled inductors and current controlled capacitors also have similar issues. Therefore, we built LC circuits with suitably chosen capacitors values along with change in the number of turns to change the inductance (Changing coil diameter requires different coils which were not available). Note that the resistors and capacitors come only in certain well-known sizes and have 1% or worse tolerance; therefore, achieving the precise resonance frequency or matching the transmitter and receiver is often a tricky and very time consuming process. We largely achieved this by trial and error.

Fig. 2: A sample MRC Antenna

There are other challenges also brought about by using the antenna on-body. Human body has a small capacitance that must be accounted for in achieving the precise resonance frequency, although this appears to remain constant. Other issues concern the quality of antenna contact with the skin and the skin properties of the person. For example, skin moisture and resistance is a function of skin hydration, humidity, temperature, and the stress level. For example, it is well known stress increases skin conductance (formally known as electrodermal activity or EDA) due to action of sweat glands, although different parts of the body have different concentration of sweat glands and hence different amount of change in conductance [26]. Similarly, skin hydration changes the conductance. Thus, the path-loss results can easily vary by a few dB or more across experiments for the same distance and frequency on the same person.

For our experiments, we asked the volunteer to either sit in a chair or stand on the lab floor. Neither mattered since the lab floor is nonconducting. We also confirmed that different postures (e.g., seated on cushioned chair with feet off the ground) did not make any difference. We measured the communication performance in two ways. First, we connected the transmitter to a signal generator and receiver to vector network analyzer (VNA) to measure the received signal. There was no common ground connection between the signal generator and the VNA, as that would invalidate the results.

For real packet transmissions, we used a pair of USRP (Universal Software Radio Peripheral) N210 boards produced by Ettus Research [27]. The boards enable flexible implementation of software radio including various type of modulation schemes along with the ability to connect different types of antennas. It includes a Xilinx® Spartan® 3A-DSP 3400 FPGA, 100 MS/s dual ADC, 400 MS/s dual DAC and Gigabit Ethernet connectivity to stream data to and from host processors. A modular design allows the USRP N210 to operate from DC to 6 GHz. In our experiments, we used BPSK modulation to study packet delivery ratio through the body at different distances.

3.1.2. Simulation Based Evaluation

As discussed earlier, real experiments must be limited to on-body case, and even in that scenario, they are inconvenient to perform on a large scale. This gap can be filled with a comprehensive simulator that supports standard methods to solve Maxwell's equations in a complex environment. Equally important is the availability of highly detailed and realistic human phantom models. There are several open source packages summarized in [28]. Unfortunately, most do not come with human phantom models. Two packages that do include them are CST studio (open source) and Sim4Life (commercial) [29]. Sim4life supports very detailed "Virtual Population" (ViP) phantom models of human body.

Realistic modeling of EM propagation through the human body requires accurate handling of surfaces with very different EM properties; therefore, numerical solutions using a fine 3D grid ("voxel") is necessary. The three main methods in this regard are [28]: Finite-differences-time domain (FDTD), Finite Element Method (FEM), and Method of Moments (MoM), or equivalently, Boundary Element Method (BEM). We have used Sim4Life FDTD method in our modeling using full Maxwell's equations (Without considering magnetostatic assumption) and thus the results should be valid regardless of the frequency. However, to avoid error accumulation due to finite differences, the voxels must be rather small in size.

As the main model in Sim4Life, the Duke, an MRI-based full-body model obtained from a virtual population, was used. The model was segmented into 75 anatomical body tissues/organs, with a resolution of 1.5 × 1.5 × 1.5 mm^3 throughout the body. The height and weight of the model were 1.77 m and 70.2 kg, respectively. Since a FEM solver is capable of operating at various frequencies, we obtained the path loss distribution with the human body model using the magneto FEM vector-potential and ultrasonic FEM solver. For USC, we used a parabolic diaphragm with specific focal point.

3.2. Intra-body Path-Loss Model

In MRC based intra-body networks, there is a need for modeling the path-loss of the communications. To fill this need we create a model using our data. The model predicts path loss for body-mounted receivers, which can be used individually or in combinations. Given a specific receiver setup (e.g., single receiver, pair of receivers, etc.), the total path loss for each receiver consists of two components:

1. A base path loss that depends on the distance from the transmitter
2. Additional losses from interactions with other active receivers (if any)

For any receiver i, the total path loss is:

$$\begin{aligned} L_{total}(i) &= L_{base}(i) + \sum_{j \neq i} L_{int}(i,j) \\ L_{base}(i) &= \alpha d_i^{\lambda} + \beta \\ L_{int}(i,j) &= \gamma d'(i,j)^{\kappa} \end{aligned} \tag{3}$$

where:

- $L_{base}(i)$ is the base path loss for receiver i incorporating distance-dependent attenuation, with d_i is the path distance (non-Euclidean) from transmitter to receiver i measured from the on-body path from transmitter to receiver.
- $\sum_{j \neq i} L_{int}(i,j)$ represents the sum of interaction effects with all other active receivers. When multiple receivers are present, each pair of receivers contributes an interaction term, with $d'(i,j)$ is the distance between receivers i and j, calculated by discretizing the body into a grid and finding the distance in terms of the path between two receivers (Note that the function is symmetric with respect to receivers i and j).

3.3. Detuning problem

3.3.1. Circuit Design

Two RLC circuits for magnetic coupling were designed. The main criteria was to have an efficient energy transfer between the two circuits at a specific frequency (13.56 MHz, which is popularly used for Intrabody MRC). The values for resistance, inductance and capacitance can be obtained from the resonance frequency and Q factor. According to [30], to have an optimal energy transfer, the coupling factor (k_{mrc}) needs to be equal to $\frac{1}{\sqrt{Q_r \cdot Q_t}}$. This coupling factor was used in the simulations. The parameter values for the RLC circuit are shown in Table 2.

Table 2: Circuit parameters

Inductance	9.27 μ H
Capacitance	14.86 pf
Resistance	50 Ω
k_{mrc}	0.063

3.3.2. Proposed Control Scheme

We model the disturbance in the transmission as a perturbation in the capacitance of the transmitter and/or the receiver since mitigating such perturbations means controlling the Q-factor and the resonance frequency (and hence the coupling factor), according to Eq. 2. The control of the capacitance can be easily swapped with that of the inductance, however, a change in inductance is generally more difficult to implement. Controlling the resistor also would not be a viable option since with resistor control, we can only manage the Q-factor, not the resonant frequency. Capacitance is selected because of its capacity to affect both objectives: achieving high Q-factor and resonance.

Fig. 3 shows our system with energy transmit and receive nodes, denoted as N_T and N_R respectively. We assume a bidirectional communication path and hence the data can flow from N_R to N_T. For controller design, we exploit the fact that the current in N_R circuit goes down whenever the two circuits do not resonate, as seen in Fig. 1. Hence, the key part of the controller is to find out which part of the curve we are on. Let $t = 1, 2, ...$ denote the time instants when the samples are taken and C_t and I_t the capacitance and the current respectively at time t. To design the controller, a truth table is constructed for the controller's behavior based on the following equations:

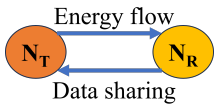

Fig. 3: System Illustration

$$\begin{aligned} \delta &= \text{Sign}(C_{t-1} - C_{t-2}) \\ \Delta_1 &= \text{Sign}(I_t - I_{t-1}) \\ \Delta_2 &= \text{Sign}(I_{t-1} - I_{t-2}) \end{aligned} \tag{4}$$

Where Sign() is the sign function. first equation in 4 describes the direction of capacitance change between $t-1$ and $t-2$. Similarly, second and third equations in 4 describe the direction of current change. Note that the controller acts at time t (the output of the algorithm is C_t) by tracking the auxiliary states described in the above equations.

In every instance, the controller acts according to three data flows it receives: current and action from one and two time sample before, and the time. For N_R, it is a matter of recording the data it already observed, and for N_T, this data is sent from N_R. We construct a truth table for each case of δ, Δ_1 and Δ_2.

Since there are two controllers on both N_T and N_R, the operation of each controller should be scheduled to prevent any interference. Each controller is given a time interval to act (Duration of controller's turn), in which the controller figures out whether it should turn on and the direction it needs to act. In each interval, the controller starts by checking the current. If it is less than the reference by more than the amount of ϵ, the controller's first action is to implement an initial increase ($W'\Delta$) in the capacitor. Using this initialization the controller figures out which direction to select using the truth table. Controller time counter (t') is a simple counter that in each turn of the controller starts from 0 and increments by 1 with each time sample until its turn is finished. A decreasing weight ($(W)^{t'}$) is given to each control signal the controller wants to implement in capacitance to keep the action selection convergent (Each turn if the controller wants to take action, after the initialization it would produce a time series $\{W^0, W^1, \ldots\}$). In Adaptive Step Controller there are multiple choices for the controller to select, based on how severe the situation is. Controller Scaler is designed for this situation for the controller to be able to act more aggressively.

It can be observed that the algorithm always picks an action that maximizes the current and consequently the efficiency, until it converges to an ϵ-optimal current. Since the current is a unimodal function of frequency, as it can be seen in Fig. 1, it must converge.

Alg. 1: Adaptive Step Controller Pseudocode

Observations: I_t := N_R Current at time t; C_t := Capacitance at time t
Parameters: W' := Initialization weight; W := Weight; ϵ := Threshold; Δ := Step size; α := Direction; $\delta = Sign(C_{t-1} - C_{t-2})$; $\Delta_1 = Sign(I_t - I_{t-1})$; $\Delta_2 = Sign(I_{t-1} - I_{t-2})$; γ:= Control Scaler=2; t'=Controller time counter
Output: C_t
Algorithm:
If NOT Controller's Turn **Then** $C_t \leftarrow C_{t-1}$
Else {
  If $|I_t - I_{ref}| < \epsilon$ **Then** $C_t \leftarrow C_{t-1}$
  Else {
    if t=1 (First round) **Then** *Initialization* $C_t \leftarrow C_{t-1} + W'\Delta$
    Else {
      $\alpha \leftarrow$**Table Look-up**$(\delta, \Delta_1, \Delta_2)$
      if $\epsilon \leq |I_t - I_{ref}| < 2\epsilon$ **Then** $C_t \leftarrow C_{t-1} + W^{t'} \cdot \alpha \cdot \Delta$
      Else {
        If $2\epsilon \leq |I_t - I_{ref}| < 4\epsilon$ **Then**
        $C_t \leftarrow C_{t-1} + \gamma W^{t'} \cdot \alpha \cdot \Delta$
        Else $C_t \leftarrow C_{t-1} + \gamma^2 W^{t'} \cdot \alpha \cdot \Delta$
    $t' = t' + 1$
}}}}
Table Look-up$(\delta, \Delta_1, \Delta_2)$:

δ	+1	-1	-1	+1	-1	+1	+1	-1
Δ_1	+1	-1	-1	+1	+1	-1	-1	+1
Δ_2	-1	+1	-1	+1	-1	+1	-1	+1
α	+1	+1	+1	+1	-1	-1	-1	-1

4. Results and Discussion

4.1. Comparison of Measurement and Simulation Results

We next ran Sim4Life for several conditions similar to real measurements. Note that the Duke model in Sim4Life does not directly represent the characteristics of any of the volunteers and thus achieving the same path length through the body and the same positions on the body is not possible. Nevertheless, our extensive measurements in [2] indicate that the differences should not be significant. Fig. 4 shows the comparison for a wide range of frequencies from 3 MHz to 50 MHz.

It can be seen that in most cases, there is a very good match between the two. In all cases, the measured loss is larger than the simulated one which could be explained by the fact that the simulated situation is ideal (there is no issue of skin-contact quality, field leakage outside the body, or even the minor loss of signal between the measuring equipment and the measured signal on the body). Accounting for this, will perhaps show an even better match. We found such a match in all the other (unreported) cases as well. The somewhat variable difference between measured and simulated values can be attributed to various sources of variations including: (a) body-type of the volunteer vs. that of the phantom, and (b) difficulties and practical issues in setting the precise values of L and C in each case, as mentioned in section 3.1.1 (c) unmodeled issues in the simulations. A consistently good match provides us some assurance on both the simulations done via Sim4Life (and corresponding ViP body models) and the accuracy of our real experiments with volunteers. Note that the experiments can be affected due to parasitic capacitances, unknown ground paths, measurement errors, etc. The most interesting result from Fig. 4 is the "sweet-spot" for the frequency even in a rather limited range of 2-50MHz. In the figure, the path-loss is minimum around 25MHz and increases on both sides. The analytical model for magnetic resonance propagation through the air cannot explain such a behavior. We believe that this is a result of frequency dependent permittivity and conductivity as illustrated in Table 1. The frequency at which the minimum occurs depends on several parameters as discussed later, and should not be construed as fixed. Even more significant, the actual values of path-loss very much depend on the Q-factor of the coils. In Fig. 4, the Q-factor is quite high (210 at 25 MHz), which is difficult to maintain for long term operation as discussed in section 2.1. If we bring Q down to 100 or lower, the path-loss would likely increase by another 10dB. Another issue is that the Q-factor will change with frequency because of practical difficulties in maintaining the same L/C ratio. However, the experiments do suggest that the behavior remains intact.

4.2. USC vs. MRC

Next we report results from some simulations, performed using both USC and MRC for 3, 5 and 8 MHz frequencies. We chose three different parts of the body, On-Body (OB) and In-Body (IB): 1. Right-lower Calf (RLC) to Left-Lower Calf (LLC), 2. Right-upper Calf (RUC) to Right-upper Calf (LUC), and 3. Right Waist (RW) to Left Waist (LW). The results are shown in Table 3. As it can be seen, the path loss for MRC is less than the path loss for USC in this frequency. Next, we compare the simulation vs. measurement results for MRC and USC at 3, 5, and 8 MHz frequencies. Table 3 also shows the comparative path-loss while at a distance of 20 centimeters. These results again show a good tracking of simulation vs. measured results for both MRC and USC.

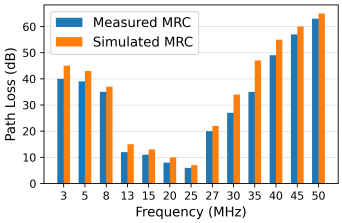

Fig. 4: MRC measured & simulated pathloss vs. freq.

It is also seen that in this frequency range, USC performs better than MRC and the path-loss goes down with frequency. For USC, this behavior is contrary to its fundamental equations, where the pressure at a given distance supposed to go down exponentially with the frequency. For MRC, the range increases with the frequency, since higher frequency implies higher energy. However, the in-air behavior of power (going down as sixth power of distance) clearly does not hold. A higher water content in the body might be helping ultrasonic waves to achieve more extended range. However, further exploration of physics is necessary to substantiate this claim. In our experiments we used diaphragm USC transducers where the diaphragm thickness goes down with frequency. We were unable to get transducers with operating frequencies > 8 Mhz.

Table 3: In-body and On-body Simulations at 13.56 MHz

TX position	**RX** position	**Dist.** (cm)	**USC PL (dB)** IB	OB	**MRC PL (dB)** IB	OB
RLC	LLC	15cm	12	14	9	11
RUC	LUC	20cm	14	15	12	13
RW	LW	36cm	17	21	12	14
Freq(MHz)	**Sim(USC)**	**Meas(USC)**	**Sim(MRC)**		**Meas(MRC)**	
8	32	35	39		37	
5	35	39	38		43	
3	37	40	39		45	

4.3. Further Simulation Studies of MRC

Having obtained some confidence in the simulation results, we conducted more extensive simulations, largely focusing on MRC. In particular, we explored the potential difference between in-body vs. on-body placement of the antenna. Fig. 5a shows the comparison of in-body vs. on-body results. It is seen that the MRC path loss is higher for frequencies up to about 10 MHz, and beyond that the difference between the two is very small; in fact, at the typical MRC frequency of 13.56MHz, MRC has slightly lower loss, and at higher frequencies the difference is negligible. It is seen that the difference between on-body and in-body scenarios is rather small, with on-body showing a slightly higher path-loss.

We further studied the behavior of MRC with frequency when the number of turns of the coil are changed. Fig. 5b shows the behavior of 20mm coil for 3, 5, and 7 turns. The results are generally expected – the path-loss decreases with the number of turns.

One thing not obvious is slight shift to the left with increasing number of turns. This behavior has been reported in [31] and is again not expected in a homogeneous media like air.

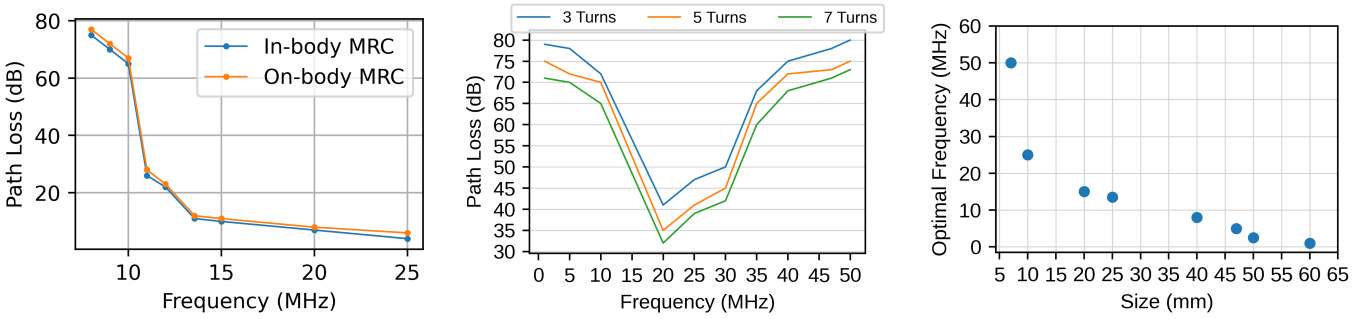

(a) (b) (c)

Fig. 5: (a) MRC simulation result for in-body and on-body cases (b) Simulated Path loss vs. frequency for different # of turns in coil (c) Optimal frequency of operation vs. coil diameter for 7-turn coil

Given the "sweet-spot" behavior of path-loss vs. frequency, we decided to examine optimal frequency as a function of coil size for MRC. The result is shown in Fig. 5c. It is seen that there is a consistent decrease in optimal frequency as the coil size increases. Please note that these results were obtained by trial-and-error, since there is no equation to indicate the optimal operating point, therefore, the results are approximate. Further approximation errors can be expected due to variation in the Q-factor. To keep the same Q-factor, the ratio of L to C would need to be maintained the same; however, this is difficult to do as explained in section 3.1.1.

Our exploration suggests that the signal propagation behavior through the human body is quite different than in a homogeneous nonconducting media like air. The results are also markedly different than are often observed with idealized modeling of body with average dielectric parameters or by considering tissues of only one type. Our results are, however, consistent with those reported in [31] and [32]. Other researchers have also reported variations in channel gain as a function of frequency for both MRC and USC [11, 7]. However, the complexity of the body and different frequency ranges, dielectric property assumptions, etc. make a direct comparison difficult.

Table 4: Transmission Efficiency

Temperature (°)	Pathloss (dB)
10	16.60
15	16.14
27	16.31
35	14.91
40	16.69

4.3.1. Skin Temperature vs. Transmission Efficiency

Our first experiment examined the energy transfer efficiency with respect to the skin temperature. For this, we increased and decreased skin temperature in the left arm and measured the efficiency. A common rubber bottle was used as the heating/cooling agent. The bottle was placed on the arm, between the two sensors, removed after 2 minutes to avoid any extended impacts, then the received power was measured. The experiments were done at 5 different temperatures, $10°$, $15°$, $27°$, $35°$ and $40°$ Celsius. As can be seen in Fig. 6.a, there is less than 1.78 dB loss between maximum and minimum measured dB loss and no apparent correlation between the temperature and efficiency is observed.

4.3.2. Blood Pressure vs. Transmission Efficiency

In the second experiment we measured the blood pressure (both Diastolic and Systolic) and efficiency. The measurements were done at different times of the day and after different activities, resulting in a range of numbers for BP. As can be seen in Fig. 6.b, there is approximately 8 dB difference between maximum and minimum measured dB loss and it changes rather drastically. Although our experiments may not present a direct correlation between BP and efficiency, we can see that blood pressure and possibly other body parameters affect how efficient the transmission is. Therefore, it is important to compensate for such changes automatically to keep the transmission efficiency high. The proposed control scheme attempts to address the need for adaptation in such scenarios.

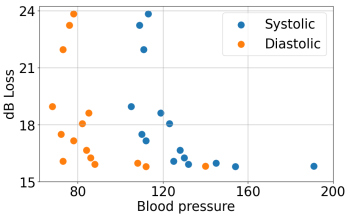

Fig. 6: a. dB Loss vs. Skin Temperature, b. dB Loss vs. Blood Pressure

4.3.3. Multi-Receiver on-body measurements

To further investigate the effect of multiple receivers on path loss, 30 experimental configurations for the receivers were created by two sets of four receivers ($\{R_{x1}, \cdots, R_{x_4}\}$ and $\{R_{x5}, \cdots, R_{x8}\}$). The locations of the receivers in the first set are on chest, left side of the waist (LW), left calf (LC), right thigh (RT), and the receivers in the second set are on placed on right arm (RA), left thigh (LT), right calf (RC) and torso.The results can be seen in Table 5. The path-loss seem to

be related to the on the body distance of the receiver from the transmitter, the distance to the other receivers, the number of receivers, and the location of the other receivers relative to each other, i.e. if receiver A is "behind" the receiver B, then there is a shadowing effect for receiver A. Another observation is that the total path-loss seems to not change much for different cases, especially in the case of multiple receivers.

Table 5: Path Loss Measurements for Different Receiver Combinations

Configuration	**Receiver Position**	P_1	P_2	P_3	P_4	P_{tot}
R_{x1}	Chest	-17.43	–	–	–	-17.43
R_{x2}	Left side of the waist	–	-19.41	–	–	-19.41
R_{x3}	Left Calf	–	–	-19.41	–	-19.41
R_{x4}	Right Thigh	–	–	–	-19.34	-19.34
$R_{x1} + R_{x2}$	Chest + LW	-18.80	-21.03	–	–	-16.76
$R_{x1} + R_{x3}$	Chest + LC	-18.27	–	-24.12	–	-17.26
$R_{x1} + R_{x4}$	Chest + RT	-19.02	–	–	-24.42	-17.91
$R_{x2} + R_{x3}$	LW + LC	–	-19.90	-23.31	–	-18.26
$R_{x2} + R_{x4}$	RT + LW	–	-19.45	–	-22.74	-17.78
$R_{x3} + R_{x4}$	RT + LC	–	–	-21.67	-20.35	-17.94
$R_{x1} + R_{x2} + R_{x3}$	Chest + LW + LC	-20.10	-22.63	-26.97	–	-17.63
$R_{x1} + R_{x2} + R_{x4}$	Chest + LW + RC	-21.04	-23.74	–	-22.27	-17.44
$R_{x1} + R_{x3} + R_{x4}$	LW + RT + LC	-20.81	–	-24.54	-23.62	-17.91
$R_{x2} + R_{x3} + R_{x4}$	Chest + LW + RT	–	-20.27	-26.74	-24.49	-18.21
$R_{x1} + R_{x2} + R_{x3} + R_{x4}$	Chest + LW + RT + LC	-21.65	-22.45	-27.32	-26.45	-17.78
Configuration	**Receiver Position**	P_5	P_6	P_7	P_8	P_{tot}
R_{x5}	Torso	-17.91	–	–	–	-17.91
R_{x6}	Right Arm	–	-18.53	–	–	-18.53
R_{x7}	Left Thigh	–	–	-19.47	–	-19.47
R_{x8}	Right Calf	–	–	–	-20.38	-20.38
$R_{x5} + R_{x6}$	Torso + RA	-19.43	-21.18	–	–	-17.21
$R_{x5} + R_{x7}$	Torso + LT	-18.98	–	-22.59	–	-17.41
$R_{x5} + R_{x8}$	Torso + RC	-18.76	–	–	-24.55	-17.74
$R_{x6} + R_{x7}$	RA + LT	–	-19.79	-21.27	–	-17.46
$R_{x6} + R_{x8}$	RA + RC	–	-19.45	–	-22.64	-17.75
$R_{x7} + R_{x8}$	LT + RC	–	–	-20.58	-21.77	-18.12
$R_{x5} + R_{x6} + R_{x7}$	Torso + RA + LT	-20.81	-22.63	-23.97	–	-17.50
$R_{x5} + R_{x6} + R_{x8}$	Torso + RA + RC	-20.86	-22.91	–	-25.29	-17.88
$R_{x5} + R_{x7} + R_{x8}$	Torso + LT + RC	-20.93	–	-23.54	-26.62	-18.33
$R_{x6} + R_{x7} + R_{x8}$	LT + RC + RA	–	-21.23	-22.73	-24.73	-17.90
$R_{x5} + R_{x6} + R_{x7} + R_{x8}$	Torso + RC + RA + LT	-21.63	-23.11	-24.51	-29.05	-17.81

4.4. Path-Loss Model Performance

The model performance was evaluated through 10-fold cross-validation (Table 6). For each fold, we computed the average absolute error by first calculating individual prediction errors for each receiver's path loss, then averaging across all receivers. The model demonstrated robust predictive capability, maintaining both training and testing errors below 2 dB across all folds. In the best-performing fold, the maximum errors were 2.85 dB for training and 1.57 dB for validation.

Table 6: 10-Fold Cross-Validation Results

	1	**2**	**3**	**4**	**5**	**6**	**7**	**8**	**9**	**10**
Training Error (dB)	1.043	1.079	1.084	1.089	1.136	1.099	1.050	1.050	1.044	1.076
Validation Error (dB)	1.359	1.089	0.986	1.007	0.415	0.850	1.309	1.351	1.288	1.184
Summary Statistics:										
Mean Training Error: 1.075 ± 0.028 dB										
Mean Validation Error: 1.084 ± 0.290 dB										
Max Training Error (Best fold): 2.85 dB										
Max Validation Error (Best fold): 1.57 dB										

4.5. Capacitive Tuning: Dual Controller Design

We implemented two controllers, a fixed step (FS) controller which only uses one fixed step size, and the adaptive step (AS) controller which can choose between three steps depending on how much current loss has happened (Alg. 1). There are three scenarios investigated in [33]: In the first scenario, the perturbation is modeled as a trapezoid with height equal to 5% of capacitance (Step Scenario), which starts and ends on both N_T and N_R sides. In the second scenario, the perturbation is modeled as a saturating ramp with a maximum equal to 5% of capacitance (Ramp Scenario), and also happens on both N_T and N_R sides. In Ramp+Step scenario, both step and ramp are present. Perturbation in both scenarios is shown in Fig. 7.

The evaluation was done using simulations using MATLAB SIMULINK toolbox[34]. For the sake of the simulations, we used two variable capacitors in parallel with the initial value of $0.5C$. The capacitance of one of these capacitors is changed according to the perturbation (Drifting Capacitance) and the other one's capacitance change with the control signal (Control Capacitance). The controller should behave in such a way that the summation of DC and CC would get closer and closer to C, and hence the resonance would be possible. In all the simulations, activation threshold ϵ and step size Δ are set as $1e^{-8}A$ and $2e^{-17}F$ for the fixed step controller. For the adaptive step controller, these parameters are set as $1e^{-6}A$ and $\{1e^{-17}, 2e^{-17}, 4e^{-17}\}$ F, respectively. Controller scaler is set to 2. For both the controllers W and W' are set as 0.9 and 1, respectively. Circuit parameters are set initially as shown in Table 2. and the voltage source is set to 1 Volt with the frequency of 13.56 MHz.

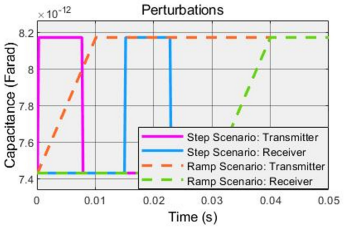

Fig. 7: Capacitance Perturbations

Ramp+Step: The scenario implements the ramp scenario with an additional 10% short-term step happening once on N_T and once on N_R. The performance of the controller can be seen in Fig. 8. The controller was able to achieve 48.83% efficiency, recovered over 99% of the maximum power and settled in the range of 0.8% of the desired capacitance.

Table 7 shows the results from actual experiments done using the circuits we designed (with different capacitances). Each experiment was done three times. Each time the temperature and blood pressure were measured to make sure they did not have any effect on the experiment. The experiments show the same trend concerning matching and non-matching circuits. The experiments show less received power which can be due to absorption of power by the body parts and power leaking to the air. Also, the coupling factor can be approximated to be 0.0495, as opposed to the optimal coupling factor calculated as 0.063 mentioned in Table 2.

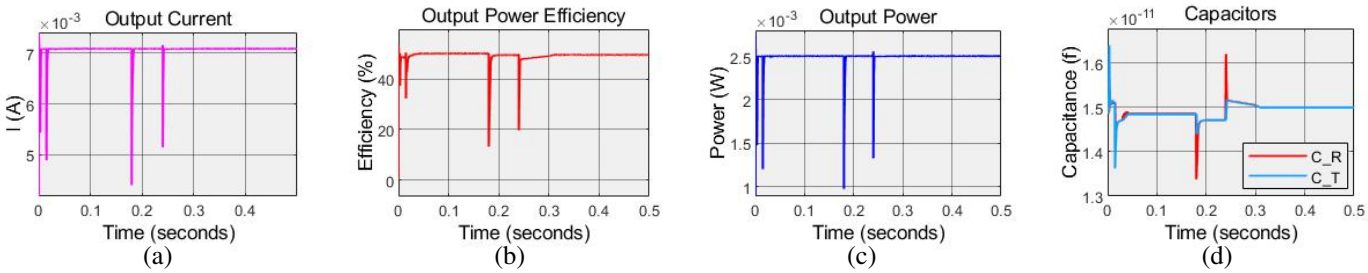

Fig. 8: **Ramp+Step Scenario**: Adaptive Step Controller Performance: a. Output current, b. Efficiency, c. Output power, d. N_R and N_T capacitances

5. Discussion

5.1. Controller Performance

The proposed Adaptive Step (AS) controller acts much better than the Fixed Step (FS) controller since it has the freedom to choose how aggressively it can behave. The sharp drops observed in current and power in the step scenario are because the perturbation pushes the circuit off the resonance rather sharply. However, the controller can bring it back to a near-optimal state. As it is observed in the ramp scenario, such drops are not experienced in current and power because the mechanism can compensate for the slow changes.

The controller can be very fast in balancing the capacitors. The convergence speed depends on the activation threshold ϵ and step size. Of course, the speed would play as an adversary to the energy efficiency of the controller and the trade-off should be studied before implementation.

One interesting observation about the difference between Fixed and Adaptive controllers is in their behavior in finding the capacitance value corresponding to the maximum power transfer. The Fixed controller behaves erratically even after reaching the optimal value and as a result, it cannot converge. The reason is that the controllers on N_T and N_R are

Table 7: Circuit Efficiency

	Recv Cap. (pF)	
Xmit Cap.(pF)	14.86	24.81
14.86	42.76%	25.32%
24.81	31.46%	39.68%

not communicating simultaneously: The controller on one side decides to move towards a direction, and ultimately missing on the optima even for a bit, then the other controller over corrects, which results in a tail-chasing behavior. In contrast, the adaptive Step controller has the option of changing the step size, hence resting at some near optimal value. The activation threshold and step size are hyper-parameters of the controller which need to be selected carefully. A low activation threshold makes the controller more sensitive to how much current loss is and hence the controller would operate more often. A high activation threshold makes the controller indifferent about how much current it can recover. Step size value would determine how big each time sample the capacitance is going to change.

Table 8: Transmission Efficiency

	Step Scenario	Ramp Scenario
Without Control	34.62%	29.33%
Fixed step	47%	48%
Adaptive step	49.54%	49.78%

The main assumption in the proposed controller is that the observable state for both controllers is the received current. That is, the controller schedule includes the communication back from N_R to N_T, which is a reasonable assumption since the control is essential only when there is communication happening. In this setting, it is reasonable to assume that the controllers on N_R and N_T are working on the same clock. However, since there is a scheduled communication and controller operation, the controllers are always working according to the schedule and each other, hence this assumption can be easily removed.

An extension could be a hyper-parameter tuning scheme inside the control loop targeting Controller Scaler according to how much improvement is obtained after each action. Implementing such tuning scheme could potentially improve the controller performance when encountering severe disturbances. Also, it should be mentioned that Alg. 1 is a three step controller, adjusting the control gain according to three levels of error. One can extend the concept of this controller to more than three steps. With appropriate scaling of intervals and parameters, it can be faster controller, in case of very aggressive and large perturbations. However, in the context of intrabody energy transfer, such severe perturbations are not expected. Hence, considering their computational cost, tuning Controller Scaler or extending the control steps, would not offer efficient solutions for such setting.

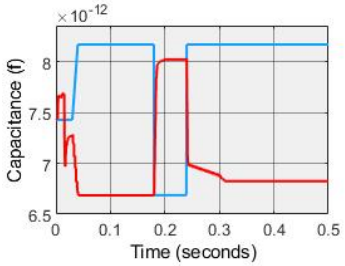

Fig. 9: N_R Capacitance Behavior in Ramp+Step

Our proposed controller has no exact matching design, but its design borrows from some of the most important algorithms. Our control drive is a PD, the weighting is the same as adaptive learning rate methods and the adaptive part uses a switching control scheme. Essentially, we expect the controller on each side to be able to mirror the disturbances on their respective sides and hence, by reversing the disturbance, diminish their effect. Such behavior is shown in Fig. 9 (red line is the control capacitance and blue line shows the drifting capacitance).

It is worth mentioning that at first, a one-sided control scheme was investigated, in which only N_T has the controller implemented on it, regardless of which side the perturbation happens. Such a controller would have been a more energy-efficient. Table 9 shows a scenario with 5% perturbation on N_R, and the controller residing on N_T. In this table, the maximum achievable value is obtained by manually changing the capacitance and finding the optimal value. As shown in Table 9, the original efficiency drops by 13% after perturbation but at best we can recover only 1% of the efficiency, meaning that using a one-sided control scheme cannot overcome the perturbation happening on the other side, leading us to investigate two-sided control.

Table 9: Performance with receive side perturbation and transmit side control

Case	I_{out}(mA)	P_{out}(mW)	Eff.
Original unperturbed value	7.08	2.51	50.0%
5% change, Before control action	6.62	2.19	36.3%
5% change, After control	6.84	2.34	37.4%
5% change, Maximum achievable	6.85	2.35	37.5%

5.2. Network-wide tuning

We now consider detuning in an intrabody network deteriorating the system performance. A rather soft assumption on drifting is, specially in clusters of nodes positioned relatively close, drifting happens the same for all the nodes, in direction, in the amount or in both. The reasoning is that drifting depends on both environmental/mechanical and physiological changes, which is the same for the nodes in a cluster, or even network wide. The main problem in link-by-link detuning in a network is that this tuning could itself cause instability when tuning different components one by one. We consider that the adaptation for tuning, happens on successive periods, meaning that controllers work in each time slot. Three main approaches can be used.

Exploiting redundancies: One approach is to add redundant sensor, to increase the robustness of the system: when a sensor drifts too much, meaning that the any attempt for control would be too expensive (e.g. the sensor node communications circuit is faulty), then the network could decide to turn it off and use another sensor of the same type for measurements (trade-off could be that

the other sensor is less accurate). In certain periods, the original sensor could be brought back online to make sure the readings of the new sensor matches. In addition, we need to use adaptive but local changes to the scheduling by reordering the communications slots in a cluster the changes needed for tuning to new frequencies minimal.

Active tuning control: We propose active control based on the proposed controller: When OBN transfers energy to the network, The nodes could be designed so that while receiving energy, the tuning controller would be active. Then assuming the OBN has a self-tuning circuit (which is relatively easy to achieve, since OBN is an On-Body Node), we can guarantee that OBN side of the communication is working in the optimal frequency. Hence the rest of the network, would be adapting to the correct value. Note that it means we would be actually implementing a one sided controller, however we are not contradicting ourselves: the one-sided controller succeeds if it is placed on the drifting side. This strategy helps significantly since every energy transfer period, the participating nodes would be recovering the optimal values for tuning.

We use the same controller structure as before, however, there are additional considerations needed here: The change in the capacitance of each receiver, affects the received current in all the other receivers, hence the observations of the controllers would not be due to their own actions. Because of this, the controllers need to take turn and cannot work simultaneously. In the following simulations, we assume 4 receivers are present, all with the same circuit parameters and coupling factor as before. The disturbance is a sharp ramp of 5% capacitance increase happening in different timings for each receiver (10ms apart). Figs. 10 to 13 show the capacitance trajectory, received power and efficiency of each receiver.

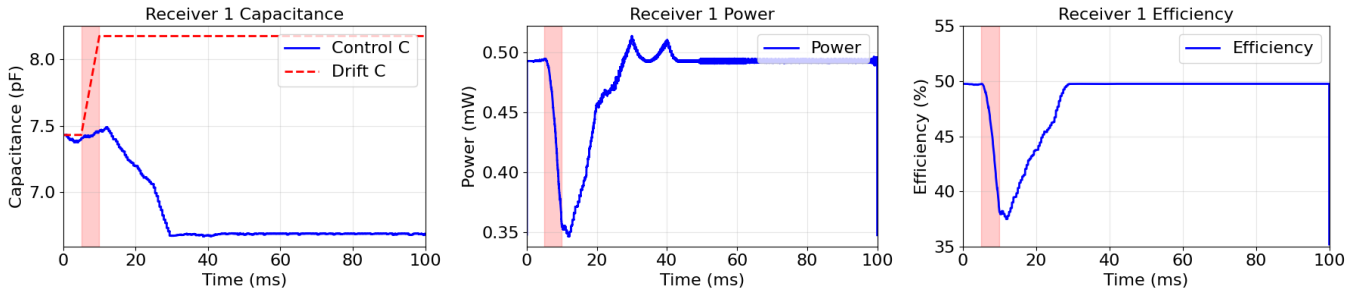

Fig. 10: Receiver 1 Control

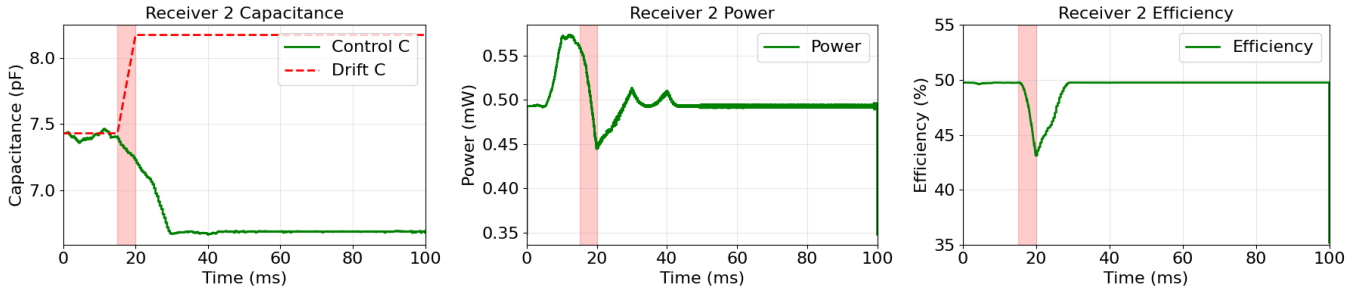

Fig. 11: Receiver 2 Control

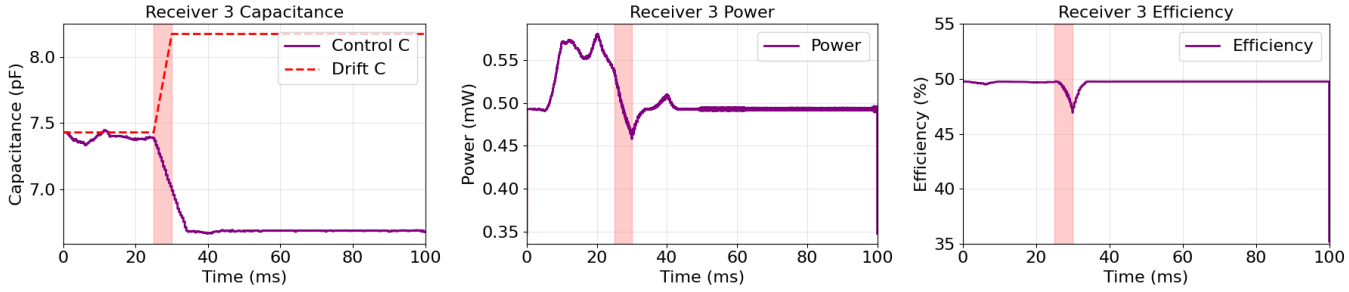

Fig. 12: Receiver 3 Control

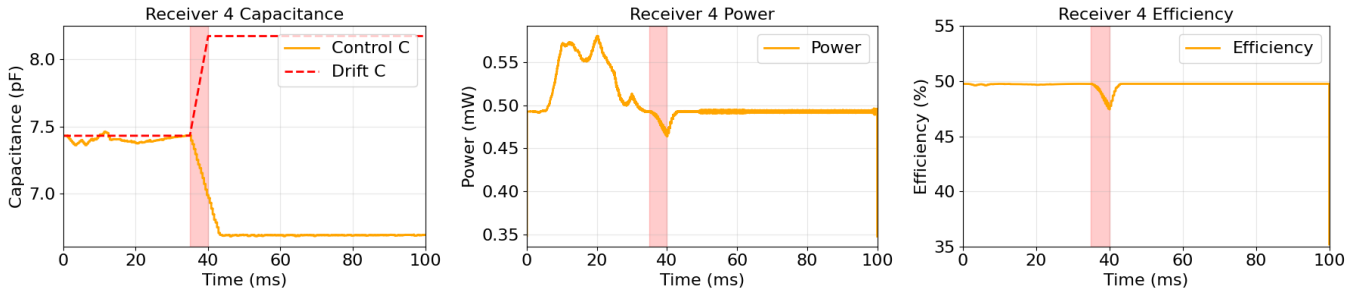

Fig. 13: Receiver 4 Control

The reason that it works is because the nodes only achieve maximum efficiency by tuning into the optimal frequency. Additionally an augmenting idea could be that instead of using energy transfer intervals to dedicated nodes, we could chop the interval into multiple pieces, hence increasing the probability of building communications between different nodes and increasing the coverage.

The reasoning behind the disturbing the capacitors is that, we argue that the human body medium, can be modeled as a complex circuit, and any changes in the path-loss (as discussed in the effect of blood pressure and body temperature) can be defined as a changed in that circuit. Our system does not try to mimic or translate the change, but look for the maximizing capacitance.

The only new issue using this method would be the coverage: consider that a cluster of a hub and a number of nodes drifted. If in the next energy transfer, only the hub was selected, then only the hub would be tuned, and now the sensors would be in a different frequency with respect to the hub. To resolve that, we could split energy transfer duration, so that it could include communications to all the nodes and the tuning would be covering all the nodes.

It should be noted that the core issue that this controller is addressing is long-term drifting, not the short-term fluctuations. Hence this controller does not need to be activated at every energy transfer, but activated sporadically.

6. Conclusions

In this paper we have examined in detail the characterization of magnetic resonance and ultrasound based communications through the human body, both via direct on-body measurements and via simulations using the Sim4Life package and its ViP phantom human body models. We show a close match between measured and simulated results in spite of many limitations of the measurements, which seems to validate our measurements. The most significant result from these measurements is that the human body does not behave at all like a homogeneous, nonconducting media like air, and thus the mathematical equations expressing the behavior in homogeneous media cannot be used to characterize the behavior through the body. The simulations and measurements provide many non-intuitive results that are difficult to explain and somewhat surprising. For example, the path-loss as a function of frequency shows a unimodal behavior, with minimum loss at a frequency that is determined by the coil size and number of turns. In the future we will explore such behavior further to understand the reasons and the impact of various factors that are difficult to control in practice.

Acknowledgements

The project was supported by the National Science Foundation (NSF) grants CNS-2129659. The authors would like to acknowledge considerable amount of measurement and simulation work done by Rajpreet K. Gulati for both MRC and USC technologies originally, and several of those results are included in this paper. The authors would also like to thank Izaz Ali (Hanyang University, Korea) for his help in obtaining Sim4Life results.

References

[1] R. K. Gulati, S. Islam, A. Pal, K. Kant, A. Kim, Characterization of magnetic communication through human body, IEEE Consumer Communications and Networking Conference (CCNC) (2022) 563–568. doi:10.1109/CCNC49033.2022.9700669.

[2] S. Islam, R. K. Gulati, M. Domic, A. Pal, K. Kant, A. Kim, Performance evaluation of magnetic resonance coupling method for intra-body network (ibnet), IEEE Transactions on Biomedical Engineering 69 (2022) 1901–1908. doi:10.1109/TBME.2021.3130408.

[3] R. Gulati, K. Kant, A. Pal, Ultrasonic vs. magnetic resonance communication for mixed wearable and implanted devices, Proc. of IEEE International Conf. on Communications (ICC) (2022) 5304–5309. doi:10.1109/ICC45855.2022.9838598.

[4] F. Akasheh, T. Myers, J. D. Fraser, S. Bose, A. Bandyopadhyay, Development of piezoelectric micromachined ultrasonic transducers, Sensors and Actuators A: Physical 111 (2004) 275–287.

[5] T. C. Chang, M. J. Weber, M. L. Wang, J. Charthad, B. P. T. Khuri-Yakub, A. Arbabian, Design of Tunable Ultrasonic Receivers for Efficient Powering of Implantable Medical Devices With Reconfigurable Power Loads, IEEE Transactions on Ultrasonics, Ferroelectrics, and Frequency Control 63 (2016) 1554–1562. doi:10.1109/TUFFC.2016.2606655.

[6] M. Abrams, Near field magnetic induction (nfmi): Dreams of wireless hearables, http://www.audioxpress.com/article/near-field-magnetic-induction-nfmi-dreams-of-wireless-hearables, 2017.

[7] E. Wen, D. F. Sievenpiper, P. P. Mercier, Channel characterization of magnetic human body communication, IEEE Transactions on Biomedical Engineering 69 (2021) 569–579.

[8] R. Shukla, N. Kiran, R. Wang, J. Gummeson, S. Lee, Skinnypower: enabling batteryless wearable sensors via intra-body power transfer, Proceedings of the 17th Conference on Embedded Networked Sensor Systems (2019).

[9] A. Kim, S. K. Lee, T. Parupudi, R. Rahimi, P. chul, Moon, Islam, Sayemul, Zhou, Jiawei, Majumdar, A. K., Park, J. S., Yoo, J. M., Ziaie, B., An Ultrasonically Powered Implantable Microprobe for Electrolytic Ablation, Scientific Reports Under review (2019).

[10] J. Park, P. P. Mercier, A sub-10-pj/bit 5-mb/s magnetic human body communication transceiver, IEEE Journal of Solid-State Circuits 54 (2019) 3031–3042.

[11] A. Ibrahim, M. Meng, M. Kiani, A comprehensive comparative study on inductive and ultrasonic wireless power transmission to biomedical implants, IEEE sensors journal 18 (2018) 3813–3826.

[12] A. Pal, K. Kant, Nfmi: Near field magnetic induction basedcommunication, Elsevier Computer Networks (2020). doi:10.1016/j.comnet.2020.107548.

[13] S. Gabriel, R. Lau, C. Gabriel, The dielectric properties of biological tissues: Ii. measurements in the frequency range 10 hz to 20 ghz, Physics in medicine & biology 41 (1996) 2251.

[14] N. Siauve, R. Scorretti, N. Burais, L. Nicolas, A. Nicolas, Electromagnetic fields and human body: a new challenge for the electromagnetic field computation, COMPEL 22 (2003) 457–469.

[15] D. Andreuccetti, R. Fossi, Proprietà dielettriche dei tessuti umani: definizioni, modello parametrico, codici di calcolo., http://niremf.ifac.cnr.it/tissprop/, 2000.

[16] J. I. Agbinya, Principles of Inductive Near Field Communications for Internet of Things, River Publishers, Wharton, TX, USA, 2011.

[17] M. Masihpour, Cooperative communication in near field magnetic induction communication systems, Ph.D. thesis, University of Technology, Sydney, 2012.

[18] I. Poole, Understanding ceramic capacitors and its types, www.electronics-notes.com, ????

[19] N. Jiang, L. Zhang, Z.-Q. Liu, L. Sun, W.-M. Long, P. He, M.-Y. Xiong, M. Zhao, Reliability issues of lead-free solder joints in electronic devices, Science and technology of advanced materials 20 (2019) 876–901.

[20] P. Si, A. P. Hu, S. Malpas, D. Budgett, A frequency control method for regulating wireless power to implantable devices, IEEE transactions on biomedical circuits and systems 2 (2008) 22–29.

[21] Y. Lim, H. Tang, S. Lim, J. Park, An adaptive impedance-matching network based on a novel capacitor matrix for wireless power transfer, IEEE Transactions on Power Electronics 29 (2013) 4403–4413.

[22] R. W. Porto, V. J. Brusamarello, L. A. Pereira, F. R. de Sousa, Fine tuning of an inductive link through a voltage-controlled capacitance, IEEE Transactions on Power Electronics 32 (2016) 4115–4124.

[23] W. Li, G. Wei, C. Cui, X. Zhang, Q. Zhang, A double-side self-tuning lcc/s system using a variable switched capacitor based on parameter recognition, IEEE Transactions on Industrial Electronics 68 (2020) 3069–3078.

[24] A. Namadmalan, Self-oscillating tuning loops for series resonant inductive power transfer systems, IEEE Transactions on Power Electronics 31 (2015) 7320–7327.

[25] R. Mai, Y. Liu, Y. Li, P. Yue, G. Cao, Z. He, An active-rectifier-based maximum efficiency tracking method using an additional measurement coil for wireless power transfer, IEEE Transactions on Power Electronics 33 (2017) 716–728.

[26] O. N. Rahma, A. P. Putra, A. Rahmatillah, Y. S. K. A. Putri, N. D. Fajriaty, K. Ain, R. Chai, Electrodermal activity for measuring cognitive and emotional stress level, Journal of Medical Signals & Sensors 12 (2022) 155–162.

[27] ettus, Ettus USRP N210, www.ettus.com/products/un210, ????

[28] M. D. Maas, Open-source electromagnetic simulation: Fdtd, fem, mom, https://www.matecdev.com/posts/differences-fdtd-fem-mom.html, 2021.

[29] S. ZMT Zurich MedTech AG, Zurich, Sim4life, https://zmt.swiss/sim4life/, 2023.

[30] J. Van Mulders, D. Delabie, C. Lecluyse, C. Buyle, G. Callebaut, L. Van der Perre, L. De Strycker, Wireless power transfer: Systems, circuits, standards, and use cases, Sensors 22 (2022) 5573.

[31] K.-W. Yang, K. Oh, S. Ha, Challenges in scaling down of free-floating implantable neural interfaces to millimeter scale, IEEE Access 8 (2020) 133295–133320.

[32] C. Han, L. Kong, Q. Li, S. Yu, Z. Zhang, J. Mao, The wireless power transmission on the wrist-to-forehead path based on the body channel, JOURNAL OF BEIJING INSTITUTE OF TECHNOLOGY 31 (2022) 91–100.

[33] H. Kia, K. Kant, Autotuning of resonant magnetic induction communications, in: 2024 20th International Conference on Distributed Computing in Smart Systems and the Internet of Things (DCOSS-IoT), IEEE, 2024, pp. 195–202.

[34] MATLAB, version: R2019b, The MathWorks Inc., Natick, Massachusetts, 2019.